1

History, Some Basics, and an Outlook

Hellmut Haberland

University of Freiburg, Department of Physics and Materials Research Institute, Stefan-Meier-Strasse 19, 79104 Freiburg im Breisgau, Germany

Anyone who has never made a mistake has never tried anything new.
A. Einstein

1.1 Introduction

A smoking fire or the formation of clouds is a naturally occurring phenomenon, which is due to *gas aggregation* of molecules. A special type of cloud will be discussed here, as it illuminates two of the concepts necessary to understand the gas aggregation sources discussed in this book. Figure 1.1 shows the mechanism of how a cloud of the type *altocumulus lenticularis*[1,2] is formed. A wind – containing some moisture – blows over a high mountain. The air rises, expands, and thus cools. Poisson's law[2,3] for an adiabatic expansion shows that a decrease in pressure (P) leads also to a decrease in gas temperature (T):

$$T^{\kappa}/P^{\kappa-1} = \text{const.} \tag{1.1}$$

where $\kappa = 5/3$ or $7/5$ for an atom or a diatomic molecule such as N_2 or O_2, respectively. Cloud formation sets in once the temperature falls below the dew point.[2] When the air has passed the mountain peak, it drops into the valley. Air pressure and temperature increase, and the water droplets evaporate. One thus has a cloud "hanging" stationary on the top a high mountain. This observation has been known since ancient times to people living near high mountains. Several studies have shown that condensation starts around "condensation germs," which – in this case – can be dust or other impurity

1 *Altocumulus lenticularis* is Latin and means a high cloud of lens-like shape. In Europe, the wind that goes with these clouds is called *foehn*, from the German word Föhn. The simplified description given in the text is valid only if the wind is not too strong and thus no turbulences occur.
2 A good introduction into several of the problems discussed here can be found on the internet.
3 See any textbook on Elementary Thermodynamics.

Gas-Phase Synthesis of Nanoparticles, First Edition. Edited by Yves Huttel.

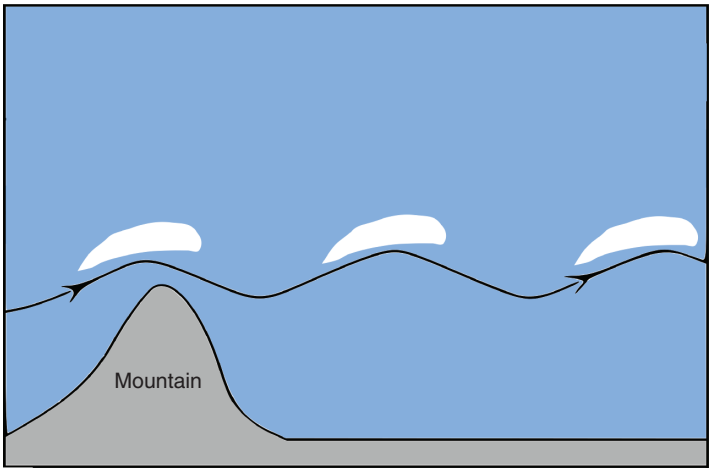

Figure 1.1 Gas aggregation is a well-known natural process: air, containing some moisture, flows over a high mountain. As the gas moves to higher altitudes, the air pressure decreases. This leads to a decrease in gas temperature; see Eq. (1.1). If the temperature is low enough, water will condense, forming a cloud. Often, a vertical oscillation of the air stream is induced by the mountain, leading to a series of stationary clouds that are produced by a moving wind.[1]

particles carried along with the wind. Two points are shown by this example: that gas aggregation

1) *needs a low temperature*, and
2) *condensation germs are necessary to start the condensation process.*

A more detailed analysis shows that the ratio of temperature to binding energy is a more relevant parameter than temperature alone; also, supersaturation controls whether the cluster grows or shrinks (see Chapter 2).

A second instructive example is the cloud chamber,[2,4] which was very important in the early days of Nuclear Physics. A mixture of air and some alcohols is exposed to a radioactive emitter, say, some α-rays. The energetic α-particles ionize the gas molecules along their path by collisions. The gas mixture is adiabatically expanded and thus cooled. The paths of the α-particles will become visible, because of the many tiny droplets condensing around the ions formed along their trajectories. The important message here is that

3) *ions are very effective condensation germs.*

These three points will be important for understanding the operation of many of the cluster sources discussed in this book. It is easy to understand why ions are so much more effective in starting a condensation than neutral atoms. The long range part of the weak interaction potential (van der Waals forces) between two neutral particles varies as R^{-6}, where R is the distance between the two particles. The interaction between an ion and a neutral atom/molecule is much stronger and of a larger range, varying as R^{-4}.

4 See any textbook on Nuclear Physics.

1.2 Three Types of Gas Aggregation Sources

Three basic prototypes of gas aggregation sources will be discussed here. Many other variants will be dealt with in the later chapters.

The *supersonic source* (Figure 1.2) has been used in many experiments for cluster studies [1–4].[5] Here, a gas, say, argon, is expanded through a small nozzle into vacuum. There are no condensation germs – if the gas is really clean – which therefore have to be produced by the expansion itself. If the expansion is strong enough, three body collisions[6] can lead to dimer formation, which will grow by subsequent collisions.

$$\begin{aligned} \mathrm{Ar} + \mathrm{Ar} + \mathrm{Ar} &\rightarrow \mathrm{Ar}_2 + \mathrm{Ar} \\ \mathrm{Ar}_2 + \mathrm{Ar} + \mathrm{Ar} &\rightarrow \mathrm{Ar}_3 + \mathrm{Ar} \\ \mathrm{Ar}_3 + \mathrm{Ar} + \mathrm{Ar} &\rightarrow \mathrm{Ar}_4 + \cdots \end{aligned} \tag{1.2}$$

For pure argon gas, the condensation germ is thus Ar_2, a weakly bound diatomic molecule, or dimer. The supersonic expansion can thus be considered as an "auto-gas-aggregation" source. Supersonic beams have intensively been used for atomic beam scattering [1–4]. Clusters of all gaseous or liquid materials can be made; even large clusters of helium have been produced. The temperature in a supersonic beam – as observed by a comoving observer with a thermometer – can become extremely small, as indicated in Figure 1.2. This is the case only if no clusters are formed. Otherwise, the heat of condensation will warm up the beam. In this case, the distribution of the internal energy of the clusters will be given by an "evaporative ensemble" [2].

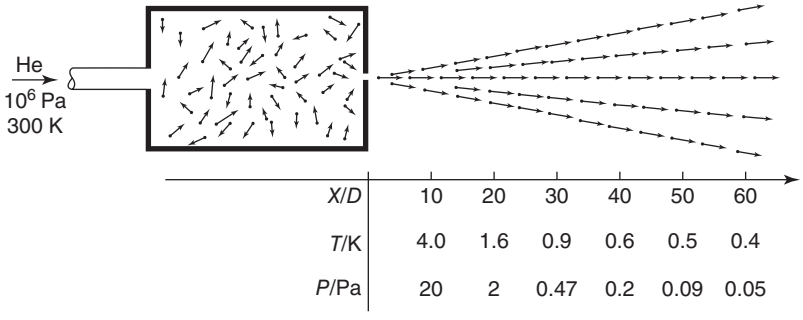

Figure 1.2 Principle of a supersonic source. Gas expands from a high pressure (say, helium at 10^6 Pa) through a small hole of diameter D into vacuum. The velocities of the He atoms are indicated by arrows. They are random in size and direction prior to the expansion. Afterward, they equalize rapidly. Temperature and pressure on the center of the beam line are given. Note the extreme cooling already close to the nozzle. A large variety of clusters have been produced using this type of "auto-gas-aggregation" source.

5 For up-to-date references, the Proceedings of the ISSPIC conferences can be consulted, for example, https://en.wikipedia.org/wiki/ISSPIC.

6 The formation of a dimer is not possible by a two-body collision, owing to energy and momentum constraints [1–4].

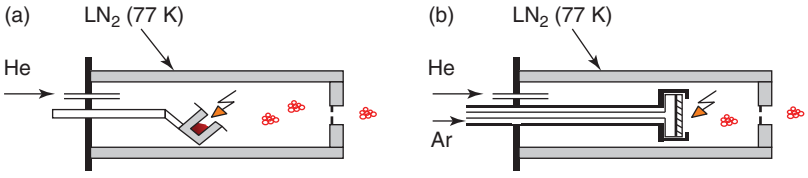

Figure 1.3 Two types of gas aggregation sources are used by the Freiburg group. Either atoms or molecules are evaporated (a) into a stream of gas; a glow discharge (indicated by the arrow) is used to produce charged clusters of both polarities. (b) The evaporator is exchanged for a magnetron sputter discharge, which does not need additional ionization.

The typical *gas aggregation source* is not fundamentally different. It obtains the low temperature necessary for particle formation by externally cooling the gas, into which some other material is evaporated or sputtered. As shown in Figure 1.3, a small stainless steel cup contains the material to be evaporated, say, sodium. The cup can be heated; Na atoms evaporate and will form neutral clusters. These could be ionized by electron or photon impact. It is simpler, more effective, and less expensive to use a glow discharge for ionization. Stable beams of neutral, positively, or negatively charged clusters could be produced and used for cluster spectroscopy. Figure 1.3b shows schematically a magnetron head, where some material is not evaporated but sputtered into the cold gas stream. Both sources have been used intensively by the Freiburg group,[7] both for cluster spectroscopy – not to be discussed here – and for thin film formation, as outlined subsequently.

Gas aggregation is a rather old technique. It was first used in 1930 to produce a film of bismuth particles used as an optical filter [5]. Broida and coworkers used it in 1971 to study the plasmon absorption of large sodium clusters [6]. Granqvist and Buhrman [7] were the first to make an analysis of the aggregation process. This author had profited a lot from discussions with Schulze in Berlin [8]. Other interesting developments were pursued in the laboratories of Sattler in Konstanz [9], Bréchignac in Paris [10], Bowen in Baltimore [11], and many others (see Chapter 3). All these groups evaporated some material into a continuous gas beam. The Smalley group [12] used instead a pulsed laser to inject laser-ablated material into a pulsed gas stream, producing a pulsed cluster beam. Reviews of cluster sources can be found in [1–4, 13].

1.3 Development of the Magnetron Cluster Source

The group of Tagaki and Yamada of the University of Kyoto had earlier published the idea to use energetic clusters for thin film formation [13, 14]. Beautiful thin films have been produced by this group, which had called their method ICB, short for Ionized Cluster Beam deposition. Unluckily, it turned out that they had no or only very few clusters in their beams. It is not known why good films were sometimes produced [14]. The experiments have been discontinued [14], and the ICB

7 For a list of publications of the Freiburg groups on (i) cluster spectroscopy and (ii) deposition studies see here: http://cluster.physik.uni-freiburg.de/issendorff_e.html.

sources are no longer available commercially. But their initial idea was correct, namely, that unusual and good thin films can be obtained by depositing energetic cluster ions.

The magnetron sputter discharge has also been known since a long time and has been routinely used in thin film formation [15, 16].[2] Magnetron sputter sources have been commercially available for many years, and for a large range of applications, for example, from small units for ultrahigh vacuum (UHV) experiments to several meter broad units used for plating of glass windows.

The author gave a series of lectures at the University of Kaiserslautern/Germany in the winter of 1986/1987. There, two groups were using standard magnetron discharges for thin film formation,[8,9] and he is thankful for the introduction into this technology. The broad range of materials that can be sputtered and the ease of operation made it tempting to use a magnetron discharge for cluster beam production. The commercially available magnetron sources in the years before 2000 could not be operated at the high argon pressure needed for efficient cluster formation. The discharge became unstable, and contaminated nanoparticles were produced.

Help came from the Paschen law [17],[2] which had been published in 1889 (yes, 1800 ..!). It states that – among other things – if the distance between two electrodes becomes very small, no discharge between them will occur. In effect, conditions are more critical than indicated by the Paschen law, owing to the presence of a magnetic field, photons, electrons, and ions. The typical distance between the sputter target at ∼−300 V and the nearest grounded metal part is only about 0.3–0.5 mm in a standard magnetron sputter source. Today magnetron sources that can be operated over a large pressure range of 10^{-4}–1 Torr are commercially available.

It is not obvious by looking at Figure 1.4 (i) that the electric field is perpendicular to the sputter target and (ii) why sputtering is observed in these sources at all. If a voltage is applied to two parallel metallic plates in vacuum, the electrostatic potential will vary linearly between the cathode (−) and the anode (+). This changes as soon as a glow discharge is ignited; the many charged particles generated by the discharge change the linear potential dramatically. They induce a weak electric field nearly everywhere, safe very near to the cathode, where a sharp drop is observed, which is colloquially called *cathode fall* [17].[2] It is alternatively known as *cathode dark space*; the first name will be used in this chapter. Here, positively charged ions are accelerated onto the cathode. An energetic ion will first liberate secondary electrons from the cathode – which then fuel the discharge – and second, eject or sputter some of the surface material. Again, this effect was observed already in the nineteenth century. Experiment and theory show that the width δ of the cathode-fall region scales as $\sim 6\,\mathrm{Pa} \times \delta$ cm [17, 18]. At a typical operating pressure of 100 Pa, one obtains the surprisingly small value of $\delta = 0.6$ mm.

---

8 Profs. Hans Oechsner and Michael Kopnarski, https://www.ifos.unikl.de/doku.php?id=home.

9 Note, that the name magnetron is also used for microwave emitters, applied earlier for RADAR, and is still in use in most microwave ovens.

The magnetron discharge[2] [18–25] uses a special type of cylindrical magnet to enhance the sputtering rate, as shown in Figure 1.4. The magnetic field lines enter and leave the sputter target. Electrons are confined to a region where the magnetic field lines are roughly parallel to the sputter target. This gives a ring-shaped glow, accompanied by a circular region of erosion of the target [16].[8] Owing to their low velocity, the argon ions are not confined by the magnetic field. Once they diffuse near the cathode, they are accelerated onto it. There they eject electrons with a probability of ~5% and also atoms from the cathode material (~50%). The electrons are accelerated by the cathode fall and fuel the discharge. The sputtered neutral atoms are used to form clusters by gas aggregation. The sputtered positively charged atoms are returned to the cathode by the electric field in the cathode fall. A thorough analysis shows that a large percentage of the sputtered atoms is redeposited onto the sputter target [20, 21]. This can be verified by visual inspection of used targets, where redeposits can be seen by the naked eye.

For a total discharge current of, say, 200 mA, one has thus an electron current of about 10 mA leaving the cathode and a 190 mA current of mainly argon ions hitting it. From this last number one can estimate [20, 21] that the ratio of charged to neutral atoms in the discharge is about 10^{-5}. The thermal load of the discharge onto the cathode is about 50 W; it must therefore be water-cooled. The

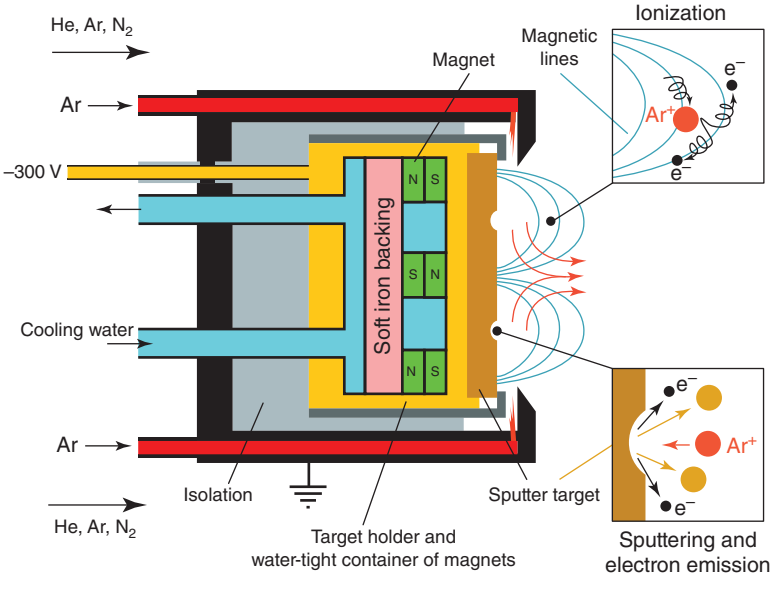

Figure 1.4 The magnetron sputter head in more detail. A cylindrical magnetic field is used. Charge production and surface erosion are maximal in the region where the magnetic field is parallel to the surface, as indicated by the two inserts. Note that the argon gas is introduced in two different regions, (i) around the source and (ii) it is blown directly into the region where sputtering is maximal. The intensity and mass distribution of clusters can be optimized, by playing with these two gas flows. The sputter head has to be water-cooled.

aggregation tube is typically cooled by liquid nitrogen, but water cooling has also been used successfully. The gas temperature just in front of the cathode has been estimated [20, 21] to be about 1000 K, with a much lower value in the downstream part of the plasma.

The first results of the Freiburg magnetron cluster source were presented at the MRS fall meeting [19] in 1990, and the source has enjoyed a growing popularity ever since. Several articles in the book show this. Two other groups had independently developed magnetron discharge sources around the same time [24]; their emphasis was on small particle formation, while the Freiburg group developed the method independently for cluster beam formation.

The plasma produced by a magnetron cluster source contains many clusters; this is – in other fields – known as *dusty plasma*. It plays an important role in interstellar space and many technologically important processes [26, 27].[2]

1.4 Deposition Machine and Mass Spectra

Figure 1.5 shows an outline of the deposition machine [19, 25] used for thin film formation by **E**nergetic **C**luster **I**mpact (ECI). It consists of six differentially pumped chambers: a chamber containing the cluster source, a deposition chamber, a load lock for rapid substrate change, an X-ray photoelectron spectrometer (XPS) for elemental analysis linked to the main chamber by a stage of differential pumping. The clusters are generated by a magnetron source (K); charged (c) and neutral (n) clusters are separated, and the charged clusters can be deposited with variable kinetic energy onto a substrate. The chemical composition of the deposited films can be studied by inner shell photoelectron spectroscopy (XPS). A time-of-flight (TOF) mass spectrometer allows measuring the size distribution of the clusters, which is relatively narrow, as can be seen in Figure 1.6. Therefore, the clusters are used as generated and not further mass selected, thus reducing the deposition time considerably. For large clusters, one observes that the positive, negative, and neutral components of the cluster beam have roughly the same intensity. Note the large fraction of charged particles, which is very much higher than that obtainable by photon or electron impact. A typical intensity – summed over all cluster sizes of one charge – is about 1 Å/s; higher intensities can be obtained, but at the cost of an inferior size distribution.

Figure 1.6 shows mass spectra of large copper clusters as a function of mass and cluster diameter. The data are well fitted by a lognormal distribution

$$f_{\mathrm{LN}} = \exp\{-\ln^2(x/x_0)/2\ln(2\sigma)\} \tag{1.3}$$

This distribution seems to be quite general, as it fits many experimental distributions. Interestingly, it can be derived in two seemingly different ways, either as a result of addition of one atom after the other [28] or by coalescence of already existing clusters [29]. Magnetron sources can produce a large variety of size distributions. Distributions with two or three maxima can be observed

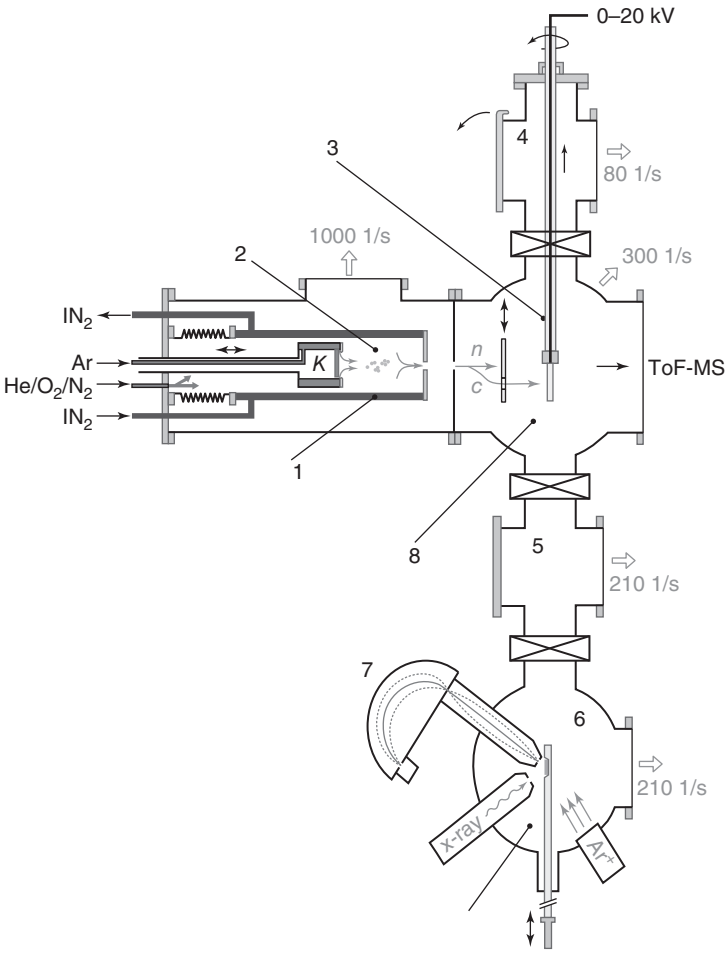

Figure 1.5 Sketch of the experimental setup. A magnetron sputter head (*K*) is sitting in the aggregation tube (1). Clusters are formed (2) in the flowing afterglow of the discharge and traverse two small holes. The beam is electrically separated into its neutral (*n*) and charged (*c*) components. Charged clusters of one polarity can be accelerated up to 20 keV and impinge in the main chamber 8 on the substrate holder (3), which can be moved horizontally by a small motor. The cluster ion beam can be swept perpendicularly to the motion of the substrate holder. A TOF-MS (time-of-flight mass spectrometer, not shown) is used for the analysis of the cluster size distribution. A load-lock chamber (4) allows rapid sample exchange. Differential pumping (5) is necessary to reach the good vacuum of the X-ray photoelectron spectrometer (XPS) chamber (6) used for *in situ* elemental analysis by an electron energy analyzer (7). Note the large pumps necessary to cope with the gas flow necessary for a gas aggregation source.

(Freiburg Cluster Group, unpublished results). But the patient experimentalist will finally arrive at a distribution as narrow as that shown in Figure 1.6, which shows a $\Delta D/D$ of only 0.2, which is not easy to obtain with other methods. The intensity quoted (~1 Å/s) could be increased considerably by using other magnetron geometries. Using a multiring cathode, for example, the intensities

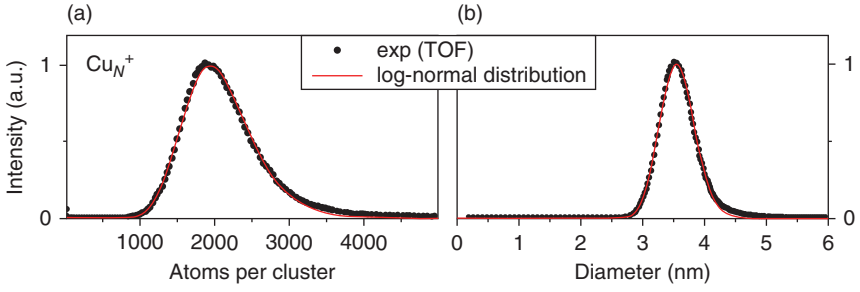

Figure 1.6 Mass spectra of large copper clusters are plotted as a function of mass (a) or as a function of diameter (b). The relative widths at FWHM (full width at half maximum) are 0.5 and 0.2, respectively. The resolving power of the mass spectrometer is not sufficient to resolve single masses for these large cluster sizes.

could be increased up to 45 Å/s, but at the expense of a much inferior mass distribution (Freiburg Cluster Group, unpublished results).

The detection of large cluster ions still presents a problem, as the probability for electron ejection from a surface scales with the velocity of the impacting particle. It rises linearly with a threshold velocity of about 50 km/s, so that very high kinetic energies are necessary for efficient single-particle detection [1–3].[2] Alternatively, one can use electric energy analyzers or even optical detection.

1.5 Some Experimental Questions

1.5.1 How Do the Clusters Start Growing?

There seems to be no intensity at low masses shown in Figure 1.6, but a more detailed study shows a lot of lines there, as shown in Figure 1.7 for cobalt clusters. The atomic and dimer ions of argon and cobalt are seen, as well as a variety of mixed clusters. It has earlier been assumed [20, 21, 30, 31] that they grow essentially by the addition of neutral metal (M) atoms:

$$M + M + Ar \rightarrow M_2 + Ar \tag{1.4}$$

The three-body rate constant for this process is

$$d[M_2]/dt = k_n\,[M]^2[Ar]$$

where [M] is the density of the sputtered metal. It is argued here that a much more effective scenario is the initial formation of the molecular ion Ar_2^+. This ion has a much larger binding energy [32][10] than the neutral Ar_2 and plays an important role is gas discharges [33]. As the density of argon atoms is much higher than that of the sputtered metal atoms, the condensation process probably starts by

$$Ar^+ + Ar + Ar \rightarrow Ar_2^+ + Ar \tag{1.5}$$

10 An antibonding electron has been removed in Ar_2^+, which together with the gerade–ungerade splitting of the potential curve leads to the large increase in the binding energy by a factor of ~125. The dissociation energy of neutral Ar_2 is 0.012 eV, which jumps for Ar_2^+ to 1.5 eV.

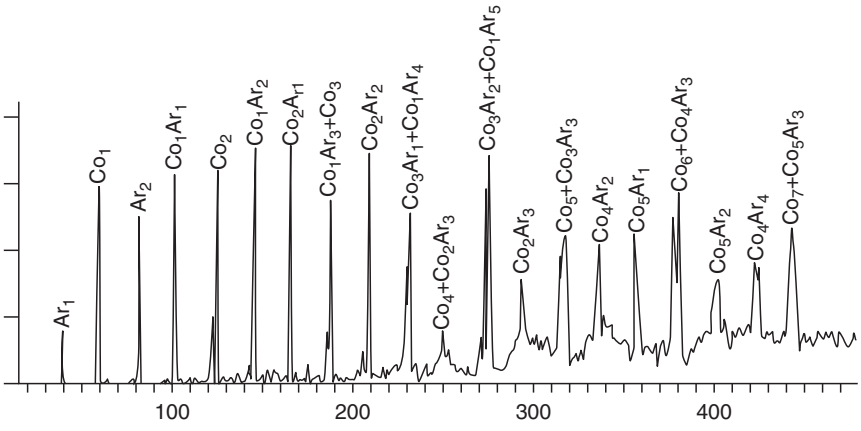

Figure 1.7 Mass spectra of small cobalt clusters taken with similar source condition used for Figure 1.6. A lot of small clusters – even atomic ions of Ar and Co – are seen, although Figure 1.6 suggests that there are no small clusters present.

The rate constant for this ionic process is similarly

$$\mathrm{d}[\mathrm{Ar}_2^+]/\mathrm{d}t = k_i\,[\mathrm{Ar}]^2[\mathrm{Ar}^+] \tag{1.6}$$

and $k_i/k_n \sim 100$, which makes the process according to Eq. (1.5) much faster than that given by Eq. (1.4). The rate constant in Eq. (1.6) is about $k_i \sim 2\times10^{-31}$ cm^6/s [20, 21], and for a pressure of 100 Pa in the aggregation tube one has $[\mathrm{Ar}] = 2.6\times10^{16}$ cm^{-3}. This gives for $k_i\,[\mathrm{Ar}]^2 \sim 100$/s. Using this one can rewrite Eq. (1.6) as

$$\mathrm{d}[\mathrm{Ar}_2^+]/\mathrm{d}t = -\mathrm{d}[\mathrm{Ar}^+]/\mathrm{d}t \sim [\mathrm{Ar}^+]/100$$

the right-hand side of which can be easily integrated. This gives a typical time constant of about 0.01 s for the ionic process of Eq. (1.5). This is much shorter than the dwell time in the aggregation tube of about 10 s. The rate constant [20, 21] of the process according to Eq. (1.4) is $k_n \sim 10^{-33}$ to 10^{-34} cm^6/s, and the number density of the sputtered metal atoms is $[\mathrm{M}] \sim 10^{13}$–$10^{14}$ cm^{-3}. This gives a time constant that significantly exceeds the dwell time in the aggregation tube, indicating that the process according to Eq. (1.4) is negligible under realistic experimental conditions.

Figure 1.7 shows mass peaks of small clusters with up to four argon atoms attached, so that the stable Ar_2^+ molecule must grow by attachment of both metal and argon atoms. A detailed analysis of this process is not available.

When the source is optimized for larger clusters, the metal cluster intensity becomes very small at about 50 atoms, only to rise for much larger sizes as shown in Figure 1.6. The particles grow and will be charged and discharged for a long time in the afterglow of the magnetron plasma, and it is envisioned that their size and charge will be influenced by the plasma properties. An analysis of these processes has been given [20, 21]. A complete treatment of the aggregation, charging, and discharging effects in the plasma of the aggregation zone is not available but has partially been discussed for dusty plasmas [26, 27].

A caveat arises from the discussion around Eqs. (1.4) and (1.5) and Figure 1.6. Even if the mass spectrum shows only very large clusters, there might be some small ones as well. These go undetected if resolution and sensitivity of the mass spectrometer are not sufficient.

It follows from the discussion around Eqs. (1.4) and (1.5) that diatomic molecules are very helpful to start the clustering process. Moreover, it is observed experimentally that a tiny flow of N_2, O_2, CO_2, and so on, introduced into the aggregation tube will lead to much larger clusters. One must therefore be extremely careful with the gas inlet system so as not to introduce impurities there. It has been found necessary for a clean system to use only stainless steel tubing in the gas inlet system; these tubes should be specially cleaned and polished on the inside. In addition, UHV-compatible flow meters, and an Argon gas purity of N6.0, that is, 99.9999% purity, should be used. Stated otherwise, the impurity level should be at most 1 ppm. Not all commercially available units comply with this strict level of cleanliness. If plastic or Teflon tubing is used in the gas inlet system, this should be regarded with extreme suspicion.

1.5.2 The Role of Sputtered Dimers

A single sputtering event will also produce some diatomic molecules and small clusters [34, 35], which could be welcome condensation germs. Typically 1% of the sputtered material is present as dimers at the low kinetic energies employed here (see the following discussion). The dimers have a broad range of internal energies, which are due to their formation process [34, 35]; this makes their destruction in the intense discharge region plausible. If they would survive the discharge, they would act as effective condensation germs. A possible exception is a very strongly bound metal, for example, niobium. It is observed experimentally that the refractory metal niobium behaves differently than metals having a lower cohesive energy, such as Al or Cu. The discharge power for an efficient cluster formation is lower by a factor of 10, and a Nb sputter target thus lives longer by a factor of 10. A possible explanation is that the sputtered dimers are not completely destroyed by the discharge. The binding energies of Nb_2 and Nb_2^+ are 5.11 and 6.15 eV, respectively [36], and thus higher by a factor of about three than those of Al_2 or Cu_2, which makes this scenario plausible.

1.5.3 Reduction of the Energy of the Impacting Ar^+ Ions owing to Charge Exchange

The target is sputtered by the impacting Ar^+ ions. These move in a background gas of about 100 Pa of neutral argon gas. The cross section of the resonant charge transfer process

$$Ar + Ar^+ \rightarrow Ar^+ + Ar$$

is in the range of 32–45 $Å^2$ for energies between 10 and 300 eV [37]. This gives a mean free path of ~0.1 mm, implying that all Ar^+ ions have made on the average six charge exchange collisions, while they are accelerated across the cathode-fall region of width 0.6 mm. For an applied discharge voltage of ~300 V, they will

impinge on the target with an average energy of only ~300/6 = 50 eV. There is very little data available on sputtering for these low impact energies.

There will also be some metal ions in the cathode-fall region. They have (nearly) no partners for a resonant charge exchange, so they will have a much higher energy. The gas around the cathode is quite hot [21], so that the density of the Ar_2^+ will not be high there. It grows only in the colder parts of the flowing afterglow [21]. Thus, only very few Ar_2^+ ions will contribute to the sputtering process.

1.5.4 Formation and Shape of the Racetrack

As stated earlier, the electric current density is the highest where the magnetic field lines are parallel to the surface. The sputtered material leaves a circular groove there, also called a *racetrack*. The width of the racetrack scales as the square root of the energetic electron cyclotron radius and therefore also as the inverse square root of the applied magnetic field [16, 18].[8] When the sputter target is new, the magnetic field is relatively low, and the cyclotron radius and thus the width of the racetrack are large. For prolonged operation, the depth of the racetrack and thus also the magnetic field become larger and larger, and the cyclotron radius consequently becomes smaller and smaller. This leads to the typical V-shaped groove observed experimentally for racetracks after prolonged operation (see Figure 2 of Ref. [38]).

1.5.5 Loss of Intensity

Only a very low fraction of the sputtered metal atoms will finally be found in the beam leaving the aggregation tube [20, 21]. This loss is due to a variety of processes:

1) About half of the sputtered metal is redeposited on the cathode [20, 21, 38]. No idea is available on how to prevent this.
2) A very large loss is due to the diffusion of the metal atoms to the wall of the aggregation chamber [20, 21], which is coated with an amorphous layer. Again, no idea is available on how to prevent this diffusive loss. (If one happens to sputter titanium, one has an additional effective pump there.)
3) Another loss happens after the exit hole of the aggregation chamber. For large clusters, this can be partially recuperated by an aerodynamic lens, as discussed subsequently (Figure 1.9).

1.6 Deposition of Clusters with Variable Kinetic Energy

Thus, an intense, continuous beam of metal clusters and cluster ions can be produced by combining a magnetron sputter discharge with a gas aggregation source. In an early experiment, molybdenum cluster ions, Mo_n^+, with n around 1200 were separated from the neutral clusters, accelerated, and deposited on a polished Cu substrate [19, 25]. Above a kinetic energy of 6 keV, highly reflecting, strongly adhering thin films are formed on room-temperature substrates. The

films can be mechanically polished, which increases the reflectivity from 95% to 97% at 10.6 μm. Rutherford backscattering spectroscopy data reveal that less than 0.5% argon is incorporated into the films. It will be discussed subsequently that the impact of an energetic cluster leads locally to a sudden increase in pressure and temperature. This tiny, high-temperature spot is formed at each impact. The high local temperature – present for several picoseconds – leads to the observed film properties. The main advantage of the method is that excellent thin films can be produced on room-temperature substrates. A large variety of thin films have been produced and analyzed with the machine shown in Figure 1.5. The following observations have been made:

1) With no acceleration, one produces porous structures, which can easily be wiped off. The kinetic energy is given by the velocity acquired on leaving the aggregation chamber [20, 21],[11] so that the kinetic energy is much lower than the cohesive energy of the cluster.
2) For increasing energy, the clusters are deformed upon impact, giving a non-compact and rather rough film.
3) If the kinetic energy is about twice the cohesive energy, compact, smooth, and well-adhering films are obtained.

Molecular dynamics simulations [39, 40] were started to understand these results; see Figure 1.8. Some caution is always appropriate when numerically simulating such large systems. The timescales of the simulation are rather short, and the interaction potential is known only approximately. Nevertheless, the simulations give a good physical insight into the process studied and are in satisfactory agreement with experiment.

The typical deposition rate is about 1 Å/s; this corresponds to a flux of about 10^{12} clusters/cm^2 s. Thus, each spot or its near surrounding is hit about every second. If the kinetic energy is high enough, the impact zone will be strongly heated and compressed. A nano shockwave is sent into the substrate. The next impact occurs only 1 s later, when this strong disturbance has died out. Thus, each deposition act is accompanied by its own local annealing. This has several positive effects: (i) very smooth and mirror-like layers are obtained, which adhere well with the substrate; and (ii) the short and very high local temperature makes unusual combination of materials possible, for example, silver layers on glass or structured Plexiglas or a shiny tungsten layer on a sheet of Teflon (Freiburg Cluster Group, unpublished results) [19, 25, 41–43]. All these films can be produced at room temperature, as each deposition step is accompanied with its own local and high-temperature annealing process. Cryogenically cooled substrates should also be possible. (iii) If a cluster arrives at a slanted surface, it will induce a downward motion of material, which leads to a self-smoothing effect [40]. (iv) Most argon atoms arriving with the cluster will evaporate owing to the high temperature after the impact, in agreement with the near-vanishing argon density in the films.

11 A numerical solution of the Navier–Stokes equation indicates that the velocity of the expanding argon stream has a Mach number below 1 (Freiburg Cluster Group, unpublished results) in agreement with the data of [20, 21].

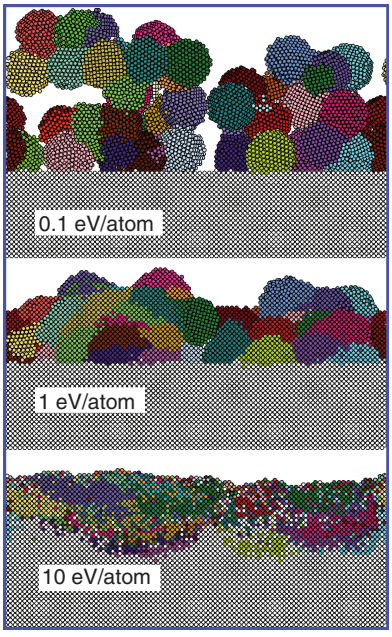

Figure 1.8 Molecular dynamics simulations of structures obtained by impact of clusters, containing 1043 molybdenum atoms each, with three different kinetic energies onto a Mo(001) substrate. At low kinetic energy, the clusters stay more or less intact after landing and form porous structures. At the highest energy, a very smooth and compact film is obtained. These results are in excellent agreement with the experimental ones.

The main properties of the magnetron cluster source can be summarized as follows:

1) The deposition rate is of about 1 Å/s, higher for very large clusters or when broad mass distributions are tolerable. Also, the addition of a tiny amount of a molecular gas (O_2, N_2, CO_2, etc.) to the sputter gas can lead to a large intensity increase.
2) The obtainable current of a cluster ion beam is a more interesting parameter for spectroscopy or scattering experiments. For very small clusters, beams of up to 1 nA have been obtained, and up to 0.1 nA for Ag_{55}^+.
3) For large clusters, typically one-third of the beams are positively or negatively charged, the rest are neutral.
4) For not too small clusters, the mass-to-charge ratio is quite low, allowing intense beams without space charge problems.
5) The cluster size can be varied over a very large range, and diatomic molecules – say, Nb_2^+ or Nb_2^- – can be produced, as well as clusters containing more than 10^6 atoms.
6) Clusters of all conductive solid materials can be made by DC sputtering. Using radio frequency (RF), nonconducting targets can be sputtered [22]. One has to be careful in this case as not to coat the ion optics with isolating material, which would lead to undesirable charging effects with ensuing ion beam instabilities.
7) Films made by clusters of high kinetic energy are very smooth and well adhering.

8) For deposition on electric isolators or of nonconducting material, intermittent neutralization of the substrate by electrons was successful (Freiburg Cluster Group, unpublished results).
9) The beam is very directed, so small holes can be filled – a problem important in the electronics industry [43].
10) A combination of points 8 and 9 allows coating highly structured PMMA (poly(methyl methacrylate)) (Plexiglas) substrates [41, 42].
11) It is easy to produce clusters from a ferromagnetic target [46] such as Fe, Co, or Ni and embed them into a nonmagnetic substrate such as Cu or SiO_2 in order to study magnetic properties of small particles.
12) The source is generally very stable with time. Instabilities are observed only for a high flux of reactive gases. In addition, the depth of the racetrack has an influence on the mass spectrum [38].
13) The source can be quickly turned on and off and does not have the long time constant of its thermal counterpart.

1.7 Outlook and Future Development

All cluster sources are presently not intense enough for most industrial thin film applications; therefore, the deposition experiments have been discontinued in Freiburg. A scale-up of the standard 2″ magnetron should be possible but leads to prohibitively large gas consumption. Future developments could proceed along the following lines:

1) Larger sputter targets, possibly with unusual geometries, and recycling of the gas.
2) Pulsed power and pulsed gas pressure have already shown some increase in the intensity.
3) Aerodynamic lenses could be used to collect much material into the beam, which otherwise would have been deposited on a wall outside the aggregation tube.

Several sputter geometries were tried (Freiburg Cluster Group, unpublished results) [19], such as two opposing magnetron heads and a cylindrical magnetron with three sets of cylindrical magnets. Higher intensities have been obtained, but at the cost of broader size distributions (Freiburg Cluster Group, unpublished results). An aerodynamic lens[2] was recently tested in Freiburg [44]; see Figure 1.9. The work is still preliminary, but intensities of up to 100 Å/s have been obtained, gaining a factor of 100 compared to the standard source.

Several problems remain unsolved:

1) The intensity has to be increased for an industrial application.
2) Only a small portion of the sputter target can be used, owing to the formation of the deep trench by the circularly confined plasma. The electronics industry has countered this problem by moving the magnets [45]. But this will probably lead to a time-dependent mass distribution [38], changing with the moving magnets.

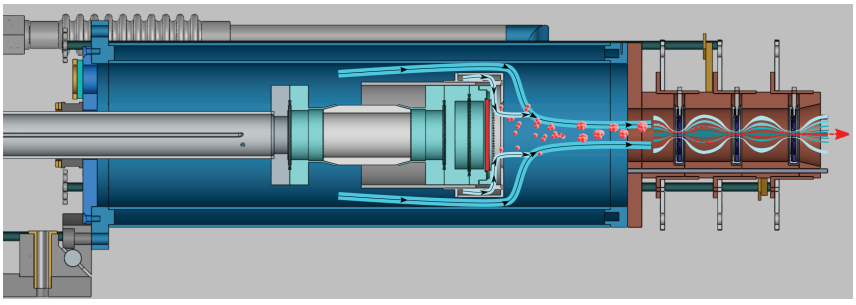

Figure 1.9 Magnetron cluster source with three stages of aerodynamic focusing. A large increase in intensity is measured for large particle sizes. The loss of intensity after the exit hole can thus be partially compensated for.

3) The majority of the sputtered atoms do not end up in the beam leaving the aggregation tube [20, 21], and no idea is presently available on how to prevent this, at least partially.
4) Although several interesting articles have appeared [20, 21, 30, 31, 38], a complete and thorough study of the aggregation and plasma processes is still missing. Moreover, it would be interesting to explore how much can be learned from the wealth of information available for dusty plasmas [26, 27].
5) The ideas and conjectures outlined in Sections 1.5.1 and 1.5.2 should be checked experimentally.

Acknowledgments

The results presented here have been obtained by several generations of students and coworkers. They are, in alphabetical order, as follows: Marga Astruc-Hoffmann, Jin-Bo Chen, Octavian Fieß, Andreas Häfele, Thomas Hippler, Zinetulla Insepov, Bernd von Issendorff, Martin Karrais, Jürgen Kraft, Markus Maier, Martin Mall, Michael Moseler, Johannes Nordiek, Daniela Olevano, You Qiang, Oliver Rattunde, Thomas Reiners, Yonka Thurner, Winnie Wolke, and Gert Wrigge. Financial support came from the European Union, the German Ministry of Research (BMFT/VDI), the German Science Foundation (DFG), the University of Freiburg/Germany, and the company Peguform/Bötzingen/Germany.

The critical reading of this introduction (or parts of it) and the constructive comments by Profs. R. Hippler, H. Oechsner, B. Smirnow, B. von Issendorff, and A. Wucher as well as by Simon Dold are gratefully acknowledged.

References

1 Scoles, G. (ed.) (1988) *Atomic and Molecular Beam Methods*, Oxford University Press, Oxford.

2 Haberland, H. (1994) *Clusters of Atoms and Molecules I*, Springer Tracts in Chemical Physics, vol. **52**, Springer-Verlag.
3 Milani, P. and Iannotta, S. (1999) *Cluster Beam Synthesis of Nanostructured Materials*, Springer-Verlag.
4 Sattler, K.D. (2011) *Handbook of Nanophysics: Clusters and Fullerenes*, CRC Press, Boca Raton, FL.
5 Pfund, A.H. (1930) Bismuth black and its applications. *Rev. Sci. Instrum.*, **1**, 397.
6 Duthler, C.J., Johnson, S.E., and Broida, H.P. (1971) Plasma-resonance scattering from small sodium particles formed in a flowing gas stream. *Phys. Rev. Lett.*, **26**, 1236.
7 Granqvist, C.G. and Buhrmann, R.A. (1976) Ultrafine metal particles. *J. Appl. Phys.*, **47**, 2200.
8 Frank, F., Schulze, W., Tesche, B., Urban, J., and Winter, B. (1985) Formation of metal clusters and molecules by means of the gas aggregation technique and characterization of size distribution. *Surf. Sci.*, **155**, 90.
9 Pfau, P., Sattler, K., Mühlbach, J., Pflaum, R., and Recknagel, E. (1982) Influence of condensation parameters on the size distribution of metal clusters. *J. Phys. F: Met. Phys.*, **12**, 2131.
10 Bréchignac, C., Cahuzac, P., Leygnier, J., Pflaum, R., Roux, J.P., and Weiner, J. (1989) Stability of alkali-atom clusters. *Z. Phys. D: At. Mol. Clusters*, **12**, 169.
11 McHugh, K.M., Sarkas, H.W., Eaton, J.G., Westgate, C.R., and Bowen, K.H. (1989) The smoke ion source: a device for the generation of cluster ions via inert gas condensation. *Z. Phys. D: At. Mol. Clusters*, **12**, 3.
12 Pettiette, C.L., Yang, S.H., Craycraft, M.J., Conceicao, J., Laaksonen, R.T., Cheshnovsky, O., and Smalley, R.E. (1988) Ultraviolet photoelectron spectroscopy of copper clusters. *J. Chem. Phys.*, **88**, 5377. doi: 10.1063/1.454575
13 Jensen, P. (1999) Growth of nanostructures by cluster deposition: experiments and simple models. *Rev. Mod. Phys.*, **71**, 1695. This review article gives a good overview on the experimental and theoretical papers on cluster deposition.
14 Yamada, I. (2016) *Materials Processing by Cluster Ion Beam, History, Technology, and Application*, CRC Press, Boca Raton, FL. See also chapter C.1 of [13], which gives a concise summary of the Kyoto ICB experiments.
15 Chapman, B. (1982) *Glow Discharge Processes*, John Wiley & Sons, Inc., New York, https://en.wikipedia.org/wiki/Sputter_deposition.
16 Ellmer, K. (2008) in *Low Temperature Plasmas, Fundamentals, Technologies, and Techniques*, vol. **2**, Chapter 26 (eds R. Hippler, H. Kersten, M. Schmidt, and K.H. Schoenbach), John Wiley & Sons, Inc., Hoboken, NJ, p. 675 (This article gives a thorough introduction into the technical basics of a magnetron discharge, as well as its application to thin film production. It should be borne in mind that the pressure is much higher and thus the cathode-fall region much narrower in the magnetron discharges discussed in this book.).
17 Ward, A.L. (1962) Calculations of cathode-fall characteristics. *J. Appl. Phys.*, **33**, 2789.
18 Wendt, A.E., Liebermann, M.A., and Meuth, H. (1988) Radial current distribution at a planar magnetron cathode. *J. Vac. Sci. Technol., A*, **6**, 1827. These

authors studied a low pressure magnetron source, but the relations cited should be applicable to the high pressure necessary for cluster formation.
19 Haberland, H., Karrais, M., and Mall, M. (1990) A new type of cluster-ion source for thin film deposition. *MRS Proc.*, **206**, 209. doi: 10.1557/PROC-206-291
20 Smirnov, B.M., Shyjumon, I., and Hippler, R. (2007) Flow of nanosize cluster-containing plasma in a magnetron discharge. *Phys. Rev. E*, **75**, 066402.
21 Kashtanov, P.V., Smirnov, B.M., and Hippler, R. (2007) Magnetron plasma and nanotechnology. *Phys. Usp.*, **50**, 455.
22 Pratontep, S., Carroll, S.J., Xirouchaki, C., Streun, M., and Palmer, R.E. (2005) Size-selected cluster beam source based on radio frequency magnetron plasma sputtering and gas condensation. *Rev. Sci. Instrum.*, **76**, 045103.
23 Mondal, S. and Bhattacharyya, S.R. (2014) Performance of a size-selected nanocluster deposition facility and in situ characterization of grown films by x-ray photoelectron spectroscopy. *Rev. Sci. Instrum.*, **85**, 065109.
24 (a) Yatsuya, S., Kamakura, T., Yamauchi, K., and Mihama, K. (1986) A new technique for the formation of ultrafine particles by sputtering. *Jpn. J. Appl. Phys.*, **25** (Part 2), L42; (b) Hahn, H. and Averback, R.S. (1990) The production of nanocrystalline powders by magnetron sputtering. *J. Appl. Phys.*, **67**, 1113.
25 Haberland, H., Karrais, M., Mall, M., and Thurner, Y. (1992) Thin films from energetic cluster impact: a feasibility study. *J. Vac. Sci. Technol., A*, **10**, 3266.
26 Walch, B., Horányi, M., and Robertson, S. (1995) Charging of dust grains in plasmas with energetic electrons. *Phys. Rev. Lett.*, **75**, 838.
27 Fortov, V.E., Ivlev, A.V., Khrapak, S.A., Khrapak, A.G., and Morfil, G.E. (2005) Complex (dusty) plasmas: current status, open issues, perspectives. *Phys. Rep.*, **421**, 1.
28 Söderlund, J., Kiss, L.B., Niklasson, G.A., and Granqvist, C.G. (1998) Lognormal size distributions in particle growth processes without coagulation. *Phys. Rev. Lett.*, **80**, 2368.
29 Villarica, M., Casey, M.J., Goodisman, J., and Chaiken, J. (1993) Application of fractals and kinetic equation to cluster formation. *J. Chem. Phys.*, **98**, 4610.
30 Kesälä, E., Kuronen, A., and Nordlund, K. (2007) Molecular dynamics simulation of pressure dependence of cluster growth in inert gas condensation. *Phys. Rev. B*, **75**, 17421.
31 Quesnel, E., Pauliac-Vaujour, E., and Muffato, V. (2010) Modeling metallic nanoparticle synthesis in a magnetron-based nanocluster source by gas condensation of a sputtered vapor. *J. Appl. Phys.*, **107**, 054309.
32 See any book on simple Molecular Orbital theory or Haberland, H. *et al.* (1991) Electronic and geometric structure of Ar_n^+ and Xe_n^+ clusters: The solvation of rare-gas ions by their parent atoms. *Phys. Rev. Lett.*, **67**, 3290.
33 Grössl, M., Langenwalter, M., Helm, H., and Märk, T.D. (1981) Molecular ion formation in decaying plasmas produced in pure argon and krypton. *J. Chem. Phys.*, **74**, 1728.
34 Wucher, A. (2007) Sputtering: experiment. *Dan. Vidensk. Selsk, Mat. Fys. Medd.*, **52**, 405.

35 Gerhard, W. and Oechsner, H. (1975) Mass spectrometry of neutral molecules sputtered from polycrystalline metals by Ar^+-ions of 100–1000 eV. *Z. Phys. B: Condens. Matter*, **22**, 41.

36 Loh, S.K., Lian, L., and Armentrout, P.B. (1989) Collision-induced dissociation of niobium cluster ions: transition metal cluster binding energies. *J. Am. Chem. Soc.*, **111**, 3167.

37 Pullins, S.H., Dressler, R.A., Torrents, R., and Gerlich, D. (2000) Guided-ion beam measurements of Ar^+ + Ar symmetric charge-transfer cross sections at ion energies ranging from 0.2 to 300 eV. *Z. Phys. Chem.*, **214**, 1279.

38 Ganeva, M., Pipa, A.V., and Hippler, R. (2012) The influence of target erosion on the mass spectra of clusters formed in the planar DC magnetron sputtering source. *Surf. Coat. Technol.*, **213**, 41.

39 Haberland, H., Insepov, Z., and Moseler, M. (1995) Molecular-dynamics simulation of thin-film growth by energetic cluster impact. *Phys. Rev. B*, **51**, 11061.

40 Moseler, M., Rattunde, O., Nordiek, J., and Haberland, H. (2000) On the origin of surface smoothing by energetic cluster impact: molecular dynamics simulations and mesoscopic modelling. *Nucl. Instrum. Methods Phys. Res., Sect. B*, **164**, 522.

41 Kleer, G., Schaeffer, E., Bodmann, M., Kraft, J., Qiang, Y., and Haberland, H. (1998) Hard and wear resistant coatings for moulding and embossing of glasses at elevated temperature. *Materialswiss. Werkstofftech.*, **29**, 545–554.

42 Qiang, Y., Thurner, Y., Reiners, T., Rattunde, O., and Haberland, H. (1998) TiN and TiAlN coatings deposited at room temperature by energetic cluster impact (ECI). *Surf. Coat. Technol.*, **101** (1-3), 27.

43 Haberland, H., Mall, M., Moseler, M., Qiang, Y., Reiners, T., and Thurner, Y. (1994) Filling of micron-sized contact holes with copper by energetic cluster impact. *J. Vac. Sci. Technol., A*, **12**, 2925.

44 Dold, S. and Issendorff, B.V., PhD thesis. University of Freiburg, Germany (to be published).

45 De Bosscher, W. and Lievens, H. (1999) Advances in magnetron sputter sources. *Thin Solid Films*, **351**, 15.

46 Qiang, Y., Sabiryanov, R.F., Jaswal, S.S., Liu, Y., Haberland, H., and Sellmyer, D.J. (2002) Magnetism of Co nanocluster films. *Phys. Rev. B*, **66**, 064404.